journal of the mechanical behavior of biomedical materials 125 (2022) 104964

Contents lists available at ScienceDirect

Journal of the Mechanical Behavior of Biomedical Materials

journal homepage: www.elsevier.com/locate/jmbbm

Research Paper

Sensitivity of the shear wave speed-stress relationship to soft tissue material properties and fiber alignment

Jonathon L. Blank [a], Darryl G. Thelen [a,b], Matthew S. Allen [c], Joshua D. Roth [a,d,*]

[a] Department of Mechanical Engineering, University of Wisconsin-Madison, Madison, WI, USA
[b] Department of Biomedical Engineering, University of Wisconsin-Madison, Madison, WI, USA
[c] Department of Mechanical Engineering, Brigham Young University, Provo, UT, USA
[d] Department of Orthopedics and Rehabilitation, University of Wisconsin-Madison, Madison, WI, USA

ARTICLE INFO

Keywords:
Finite element model
Shear wave tensiometry
Fibrous soft tissue
Probabilistic analysis
Tendon
Ligament

ABSTRACT

The use of shear wave propagation to noninvasively measure material properties and loading in tendons and ligaments is a growing area of interest in biomechanics. Prior models and experiments suggest that shear wave speed primarily depends on the apparent shear modulus (i.e., shear modulus accounting for contributions from all constituents) at low loads, and then increases with axial stress when axially loaded. However, differences in the magnitudes of shear wave speeds between ligaments and tendons, which have different substructures, suggest that the tissue's composition and fiber alignment may also affect shear wave propagation. Accordingly, the objectives of this study were to (1) characterize changes in the apparent shear modulus induced by variations in constitutive properties and fiber alignment, and (2) determine the sensitivity of the shear wave speed-stress relationship to variations in constitutive properties and fiber alignment. To enable systematic variations of both constitutive properties and fiber alignment, we developed a finite element model that represented an isotropic ground matrix with an embedded fiber distribution. Using this model, we performed dynamic simulations of shear wave propagation at axial strains from 0% to 10%. We characterized the shear wave speed-stress relationship using a simple linear regression between shear wave speed squared and axial stress, which is based on an analytical relationship derived from a tensioned beam model. We found that predicted shear wave speeds were both in-range with shear wave speeds in previous *in vivo* and *ex vivo* studies, and strongly correlated with the axial stress ($R^2 = 0.99$). The slope of the squared shear wave speed-axial stress relationship was highly sensitive to changes in tissue density. Both the intercept of this relationship and the apparent shear modulus were sensitive to both the shear modulus of the ground matrix and the stiffness of the fibers' toe-region when the fibers were less well-aligned to the loading direction. We also determined that the tensioned beam model overpredicted the axial tissue stress with increasing load when the model had less well-aligned fibers. This indicates that the shear wave speed increases likely in response to a load-dependent increase in the apparent shear modulus. Our findings suggest that researchers may need to consider both the material and structural properties (i.e., fiber alignment) of tendon and ligament when measuring shear wave speeds in pathological tissues or tissues with less well-aligned fibers.

1. Introduction

The use of shear wave propagation to measure material properties and/or loading in tendons and ligaments is a growing area of interest in biomechanics. Ultrasound shear wave elastography has been used to measure the shear modulus of passively stretched or unloaded tendon (Cortes et al., 2015)– (Corrigan et al., 2019) and ligament (Wu et al., 2020). Shear wave tensiometry is an emerging technique that is used to gauge loading in tendons and ligaments based on the speed of a shear wave propagating along the tissue (Martin et al., 2018). Using Timoshenko beam theory, we can deduce that the shear wave speed squared is proportional to the axial stress in the tissue, the density of the tissue, and the unloaded shear modulus of the tissue (Martin et al., 2018). Shear wave speeds have been shown to correlate with stress in tendon both *in vivo* (Martinet al., 2018) and *ex vivo* (Martin et al., 2019). This linear relationship has also been demonstrated in collateral ligaments *ex vivo*

* Corresponding author. 1111 Highland Avenue Room 5037, Madison, WI, 53705, USA.
E-mail address: roth@ortho.wisc.edu (J.D. Roth).

https://doi.org/10.1016/j.jmbbm.2021.104964
Received 2 August 2021; Received in revised form 26 October 2021; Accepted 6 November 2021
Available online 14 November 2021
1751-6161/

(Blank et al., 2020a).

Differences in tissue material properties may affect the relationship between the shear wave speed and axial stress. The material properties of tendon and ligament vary widely due to specimen-to-specimen or subject-to-subject differences, such as age (Woo et al., 1986), (Waugh et al., 2012), injury history (Reeves et al., 2009) or pathology (Arya and Kulig, 2010), and activity level (Reeves et al., 2003). Experimental evidence also suggests that shear wave speeds can be highly variable between specimens *ex vivo* (Blank et al., 2020a), which may reveal differences in material properties from specimen-to-specimen that are commonly observed in mechanical testing (Gardiner and Weiss, 2003). The extent to which these variations in material properties can affect shear wave propagation remains largely unexplored.

One key factor that might affect the mechanical behavior and/or material properties of tendons and ligaments is the tissue's substructure. Both tendons and ligaments are composed of longitudinal collagen fibers arranged in bundles at different scales enveloped in a ground matrix (Kannus, 2000). However, ligaments generally have less well-aligned fibers than tendon (Amis, 1998), and both healthy tendon and ligament can exhibit a collagen architecture with varying degrees of alignment (Provenzano and Vanderby, 2006). There are also several extrinsic factors that may further influence tendon or ligament substructure. For example, collagen organization is disrupted by injury in both tendon (Sivaguruet al., 2010) and ligament (Shrive et al., 1995), and healing sites in tendons are also known to have an unorganized collagen substructure following graft removal (Burks et al., 1990). Finally, interaction between the fibers and tissue ground matrix may alter the apparent shear modulus of the tissue (i.e., unloaded shear modulus determined by contributions from both the ground matrix and collagen fibers). However, it is unknown whether substructural differences alter shear wave propagation within the tissue.

We have recently developed a dynamic finite element model of shear wave excitation and propagation (Blank et al., 2020b) in a transversely isotropic tissue that includes a probabilistic fiber distribution (Gouget et al., 2012). With this model, it is possible to leverage probabilistic high-throughput computing to systematically explore a wide parameter space of both material and substructural tissue properties that is otherwise challenging to explore experimentally. Accordingly, the objectives of this study were to (1) characterize changes in the apparent shear modulus induced by variations in constitutive properties and fiber alignment, and (2) determine the sensitivity of the shear wave speed-stress relationship to variations in constitutive properties and fiber alignment.

2. Methods

2.1. Finite element model

All models/simulations were constructed/performed using the FEBio software suite (FEBio 3.0, Salt Lake City, UT). We modeled the tissue as a 60-mm long, transversely isotropic rectangular prism with an aspect ratio of 8 (width = 16 mm, thickness = 2 mm) and a similar cross-sectional area as a porcine collateral ligament (Blank et al., 2020a). The mesh was composed 0f 15,360 linear hexahedral elements with four elements spanning the thinnest dimension (Fig. 1). The mesh density was determined with an a priori mesh convergence analysis (see Supplementary material S1).

2.2. Hyperelastic model

2.2.1. Transversely isotropic material model

We modeled the tissue as an incompressible, transversely isotropic hyperelastic material that represents a material with longitudinal fibers embedded in an isotropic, Mooney-Rivlin ground matrix (Weiss et al., 1996). The ground matrix, collagen fibers, and tissue's volumetric response to loading were characterized using the following uncoupled strain energy density function, Ψ:

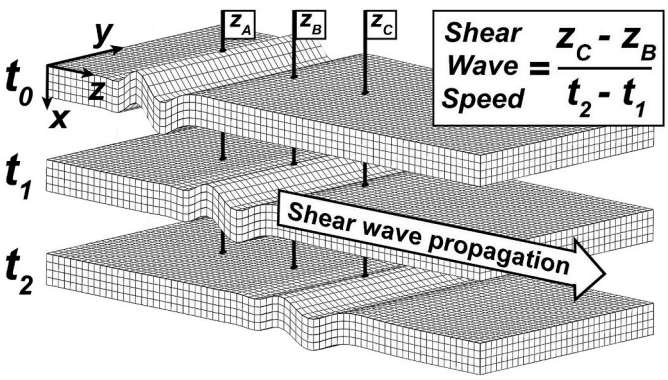

Fig. 1. Our finite element model consisted of a transversely isotropic rectangular prism with fibers oriented longitudinally (along the z-axis). The tissue was loaded to a constant strain in the z-direction. A shear wave was excited by displacing nodes (z_A) through the tissue thickness (x-axis), and the shear wave speed was computed using spacing between two nodes downstream from the excitation (z_B and z_C) and the time delay in wave arrival at those two nodes. The nominal fiber direction was the z-direction. The distribution of fiber alignment was modeled according to a two-dimensional (2D) von Mises distribution (Fig. 2) in the XZ-plane. The shear wave excitation in this figure was idealized and amplified for visualization (see Methods 2.3 for description of excitation).

$$\Psi = F_1\left(\tilde{I}_1, \tilde{I}_2\right) + F_2\left(\tilde{\lambda}\right) + \frac{K}{2}(\ln J)^2 \tag{1}$$

$\tilde{I}_1$ and $\tilde{I}_2$ represent the first and second invariants of the right Cauchy-Green deformation tensor, $\tilde{\lambda}$ indicates the deviatoric part of the stretch ratio along the fiber direction, K represents the bulk modulus, and finally J represents the volume change of the deformation. $F_1(\tilde{I}_1, \tilde{I}_2)$ represents the contribution of the ground matrix to the strain energy density function:

$$F_1\left(\tilde{I}_1, \tilde{I}_2\right) = C_1\left(\tilde{I}_1 - 3\right) + C_2\left(\tilde{I}_2 - 3\right) \tag{2}$$

The transverse tangential shear modulus of the ground matrix (and thus the transversely isotropic tissue in the unloaded state) can be estimated as $2 \times (C_1 + C_2)$. $F_2(\tilde{\lambda})$ represents the contribution of the collagen fibers to the strain energy density function:

$$\begin{aligned} \tilde{\lambda}\frac{\partial F_2}{\partial \tilde{\lambda}} &= 0 \quad \tilde{\lambda} \le 1 \\ \tilde{\lambda}\frac{\partial F_2}{\partial \tilde{\lambda}} &= C_3 e^{C_4\left(\tilde{\lambda}-1\right)} - 1 \quad 1 < \tilde{\lambda} \le \lambda^* \\ \tilde{\lambda}\frac{\partial F_2}{\partial \tilde{\lambda}} &= C_5\tilde{\lambda} + C_6 \quad \tilde{\lambda} > \lambda^* \end{aligned} \tag{3}$$

here, $\tilde{\lambda}$ represents the tissue stretch during loading, and λ^* is the stretch at which the fibers engage. Prior to this stretch level, the fibers are either slack or uncrimping, where the term C_3 scales the exponential stress and the term C_4 controls the strain-dependent rate at which the fibers uncrimp. The term C_5 corresponds to the elastic modulus of straightened fibers and C_6 is determined using the requirement that the stress-strain curve be continuous at λ^*. For a transversely isotropic material, the stretch of the collagen fibers is the same as $\tilde{\lambda}$, which is a function of deformation in the z-direction (Fig. 1). The following section will discuss the generalization of this concept to allow for an XZ-plane fiber distribution.

2.2.2. Fiber distribution model

Variation in the tissue's intrinsic fiber alignment was represented using a semi-circular von Mises distribution ('Mooney Rivlin von Mises

Fibers material in FEBio) (Gouget et al., 2012), (Girard et al., 2009), which has been previously used to model the loading response of ligaments from bovine hooves (Stender et al., 2018). The strain energy density function from 2.2.1 can be defined as the following:

$$\Psi = \Psi_{matrix} + \Psi_{fiber} \tag{4}$$

where $\Psi_{matrix} = F_1(\widetilde{I}_1, \widetilde{I}_2)$ and $\Psi_{fiber} = F_2(\widetilde{\lambda})$. The axial stress of the transversely isotropic model in response to loading was scaled using the following relationship:

$$\Psi_{fiber} = \int_{\theta_p-\frac{\pi}{2}}^{\theta_p+\frac{\pi}{2}} P(\theta,\ k_f,\ \theta_p)\ F_2\left(\widetilde{\lambda}[\theta]\right)\ d\theta \tag{5}$$

here, the two-dimensional (2D) unimodal distribution function P (θ) can be represented as:

$$P(\theta,\ k_f,\ \theta_p) = \frac{1}{\pi I_0(k_f)} e^{k_f \cos\left(2\left(\theta-\theta_p\right)\right)} \tag{6}$$

The principal fiber orientation, θ_p, represents the nominal fiber angle and was chosen to align with the longitudinal axis of the tissue (defined from positive z-axis in XZ-plane, Fig. 1). I_0 represents the modified Bessel function of the first kind. and the fiber alignment factor, k_f, determines the degree of fiber alignment within the tissue. Fiber alignment factor values from 0 to 500 were chosen to represent highly unaligned (i.e., isotropic fiber distribution) and perfectly aligned fibers, respectively (Fig. 2) (Stender et al., 2018).

The apparent shear modulus of the tissue depends on both the material properties of the ground matrix and the alignment of collagen fibers relative to the loading direction. The magnitude of the unloaded apparent shear modulus for each model was computed by loading a single element in simple shear and computing the slope of the shear stress-shear strain relationship close to a planar shear stress of zero MPa (see Supplementary material S2) (Weiss et al., 2002). This value was confirmed by comparison to the corresponding term in the spatial elasticity tensor in the transversely isotropic material model ($k_f = 500$).

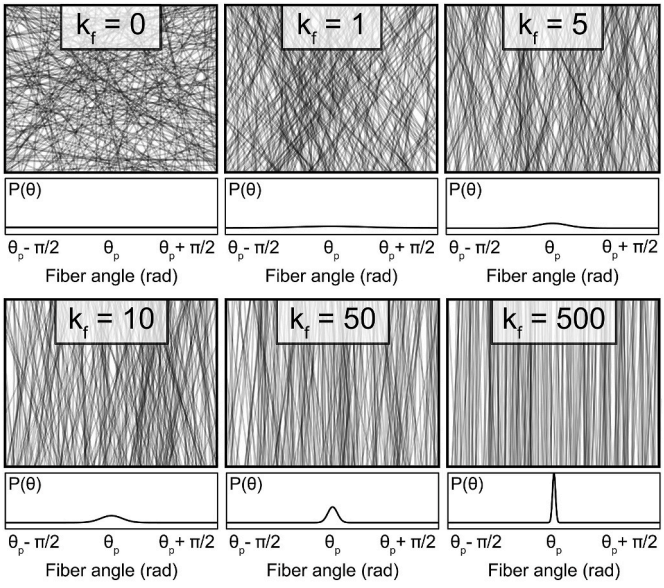

Fig. 2. Our finite element model incorporated a von Mises fiber distribution, P (θ), in the XZ plane (Eq. (5) and (6)). As shown in Fig. 1, the z-direction is the longitudinal direction (θ_p=0°) and the x-direction is through the tissue thickness. A low fiber alignment factor, k_f, corresponds to an evenly distributed probability distribution function (i.e., unaligned fibers), while a high fiber alignment factor has a probability distribution function with a high probability of fibers oriented in the preferred fiber orientation (in this case, along the z-axis). The fiber distributions shown are representative of the 2D unimodal distribution function (plots below fibers are normalized to enable visualization of the distribution). Fibers are not embedded in the model, but rather the strain energy density function is scaled to include the contribution of the fibers (Eq. (5)).

2.3. Dynamic finite element simulations

All finite element simulations were performed in FEBio version 3.0 (Maas et al., 2012). The bottom surface of the structure was held fixed. In the initial, static portion of the simulation, we loaded the model to a constant axial (z-direction) strain and allowed it to settle. The top surface of the structure was allowed to only translate in the vertical z-direction during the static portion of the simulation, but was held fixed during the dynamic portion of the simulation. During the dynamic portion of the simulation, we excited a shear wave in the model by applying a transverse displacement ramp of 20 μm over 0.62 ms to nodes through the model's cross-section (z_A, Fig. 1). The excitation displacement and timing was chosen to match the excitation signal of a piezoelectric tapper from previous *ex vivo* experiments with ligaments (Blank et al., 2020a). We monitored the velocity profile of the transverse motion at two points on the surface of the tissue located 5 and 10 mm from the excitation location (z_B and z_C, respectively, Fig. 1) to match measurement locations in previous *ex vivo* experiments (Blank et al., 2020a). We computed the shear wave speed using the spacing between measurement locations (z_B and z_C) and the time delay in wave arrival at each location, which we computed using a normalized 2D cross-correlation of the two transverse nodal displacements (Martinet al., 2018), (Blank et al., 2020a), (Cespedes et al., 1995) (Fig. 1). This technique to measure the shear wave speed was chosen to match that in previous experimental shear wave speed measurements (Martin et al., 2019), (Blank et al., 2020a).

2.4. Parametric analysis

We used a Monte Carlo modeling approach to determine sensitivities of the shear wave speed-stress relationship to model parameters. We chose ranges of constitutive parameter to cover those in previous studies using the same or similar material models (Table 1) (Martinet al., 2018), (Gardiner and Weiss, 2003), (Weiss et al., 2002), (Quapp and Weiss, 1998). The bulk modulus, K, was chosen to be a factor of 10^3 greater than the stiffness of the ground matrix to enforce incompressibility.

We created two groups of models: one with perfectly aligned fibers, and one with distributed fibers (Fig. 3). For both, we varied all constitutive parameters according to a random uniform distribution between the limits specified in Table 1. The distributed fiber model incorporated a fiber alignment factor, k_f (Eq. (5)), that was varied randomly using a one-sided normal distribution (mean = 0, standard deviation = 25). The randomly selected fiber alignment factors were all positive. We varied the applied strain, ε, in every simulation according to a random uniform

Table 1
Ranges of hyperelastic model parameters used in the Monte Carlo simulations.

Parameter	Value
Applied strain, ε [%]	0–10
Density, ρ [kg/m^3]	1000–2000
C_1 [MPa]	0.01–0.4
C_2 [MPa]	0.01–0.4
C_3 [MPa]	0.1–1.5
C_4	30–70
C_5 [MPa]	300–900
λ^* [mm/mm]	1.04–1.1
K [MPa]	$10^3 \times C_1$

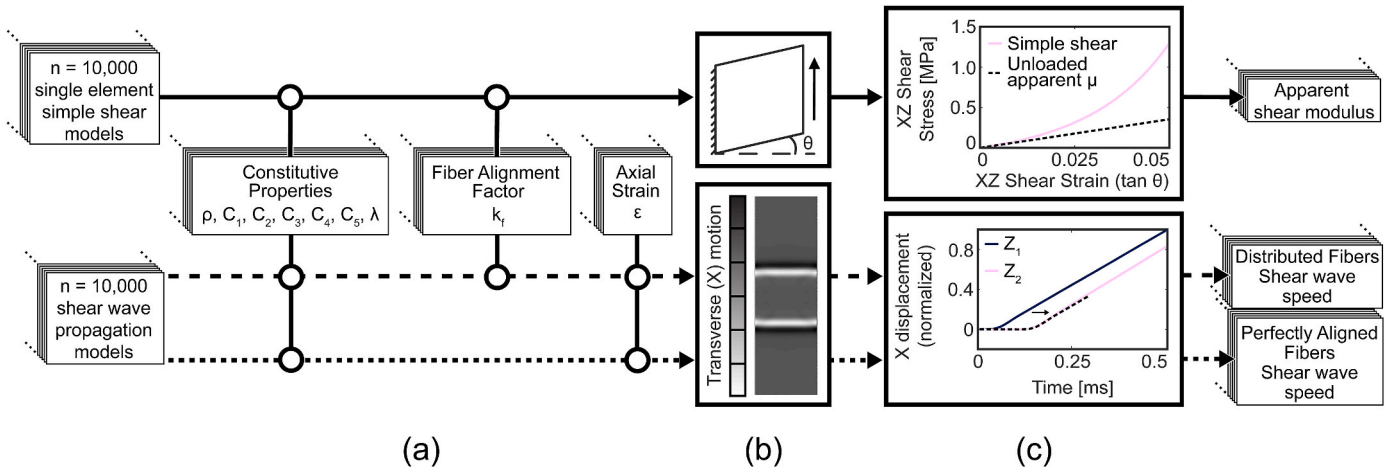

Fig. 3. (a) We varied constitutive parameters for two groups of 10,000 shear wave propagation and single element simple shear models according to random uniform distribution (Table 1). To ascertain sensitivity to fiber alignment, we incorporated a fiber distribution in the plane parallel to the shear wave excitation (Fig. 1) for one of the 10,000 model groups by randomly sampling the fiber distribution factor, k_f, according to a one-sided normal distribution. (b) We executed all simulations in parallel on a high-throughput computing grid before (c) computing shear wave speeds and apparent shear moduli (see Methods 2.3 and Supplementary material S2, respectively).

distribution ranging from 0% to 10% strain. To access a wide parameter space, we generated 10,000 unique models per group using a custom Python script. All models were executed using FEBio v3.0 on compute nodes in parallel using a high-throughput computing grid.

2.5. Statistical analysis

For our first objective, we evaluated the relationship between changes in model parameters and changes in the apparent shear modulus. We first binned the models based on the fiber alignment factor, k_f (i.e., one bin for $k_f = 0$, one bin for $k_f = 1$, etc.). Within each bin, we performed simple linear regressions between chosen constitutive properties (independent variables) and the apparent shear modulus (response variable). We also performed this analysis using the shear modulus of the ground matrix (i.e., $2 \times (C_1 + C_2)$) as an independent variable (see Section 3.2).

For our second objective, we evaluated the sensitivity of the shear wave speed-stress relationship to constitutive properties and fiber alignment in our three-dimensional finite element model. The squared shear wave speed-stress (c^2-σ) relationship is based on a one-dimensional tensioned beam model (Martinet al., 2018), (Timoshenko, 1922), (Timoshenko, 1921), which states that the axial stress in a tissue (i.e., tendon or ligament) under tension can be estimated using the following relationship (Martinet al., 2018):

$$\sigma = \rho c^2 - k'\mu \tag{7}$$

here, c is the shear wave speed, σ is the axial stress, μ is the apparent shear modulus tangential to the loading direction, k' is a shear correction factor ($k' \approx 0.822$ for a rectangular cross-section (Dong et al., 1651)), and ρ is the effective density of the model. We first grouped the results into 40 separate bins between the minimum and maximum prescribed value (Table 1) of the corresponding constitutive parameter (i.e., 40 bins for C_1, 40 bins for C_2, etc.). Within each bin, we performed simple linear regressions between the squared shear wave speed and the axial stress (Cauchy Stress T_{zz}, Fig. 1). We performed this same analysis to models grouped by 50 separate bins corresponding to the fiber alignment factor (i.e., one regression for $k_f = 0$, one for $k_f = 1$, etc.). The fitted slope of the linear regression (ρ_A) theoretically corresponds to the tissue density, and the fitted intercept of the linear regression ($-k'\mu_A$) should represent the apparent shear modulus of the tissue in the unloaded state (Eq. (7)). We then evaluated the sensitivity of the fitted slope or intercept (response variable) to the entire range of constitutive properties and fiber alignment (independent variable) by performing a simple linear regression (see Section 3.3).

3. Results

3.1. Comparison to analytical model

Shear wave speeds from both model groups increased monotonically with the axial stress. For the models with perfectly aligned fibers ($k_f = 500$), finite element model-measured shear wave speeds were within the upper and lower bounds of our tensioned beam model, which were defined using the extrema of the model densities and ground matrix shear moduli (Fig. 4). However, when distributed fibers were represented, the simulated shear wave speeds shifted to higher values that exceeded the upper extrema of shear wave speeds predicted using the tensioned beam model (Eq. (7)).

3.2. Changes in apparent shear modulus

The presence of off-axis fibers modulated the apparent shear modulus of the tissue. For highly aligned fibers (i.e., high k_f), the apparent shear modulus converged to the shear modulus of the ground matrix. However, unaligned fibers (i.e., low k_f) dramatically elevated the apparent shear modulus of the unloaded tissue (Fig. 5). Our regression analysis revealed that the ground matrix properties (C_1, C_2)

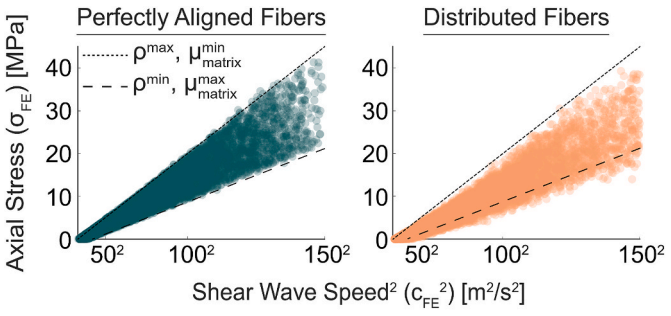

Fig. 4. Shear wave speeds measured using the finite element model increased with increasing axial stress. When fibers were perfectly aligned, these shear wave speeds fell within the bounds of our analytical model.

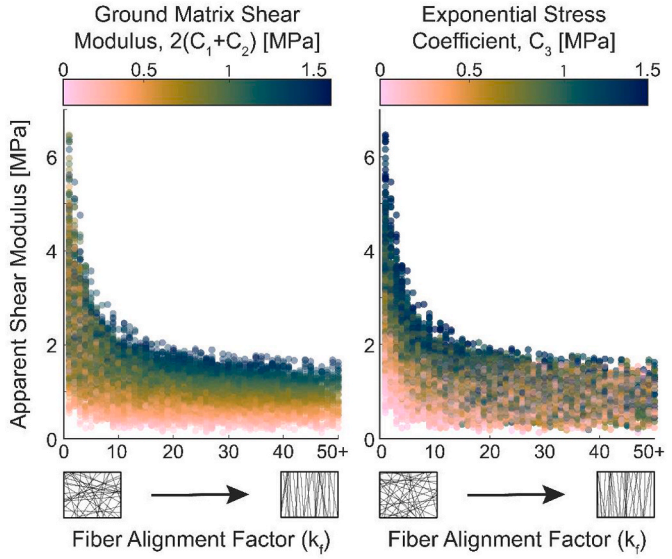

Fig. 5. (left) For the distributed fiber model, the unloaded apparent shear modulus of the tissue decreases with increasing fiber alignment and converges to the shear modulus of the ground matrix for sufficiently highly-aligned fibers. (right) The fiber exponential stress coefficient, C_3, causes an increase in the apparent shear modulus when fibers are less well-aligned ($k_f < 6$), but not when fibers were sufficiently highly aligned. We used a scientifically derived color-map to better enable visualization with regard to color-vision deficiencies and color-blindness (Crameri et al., 2020).

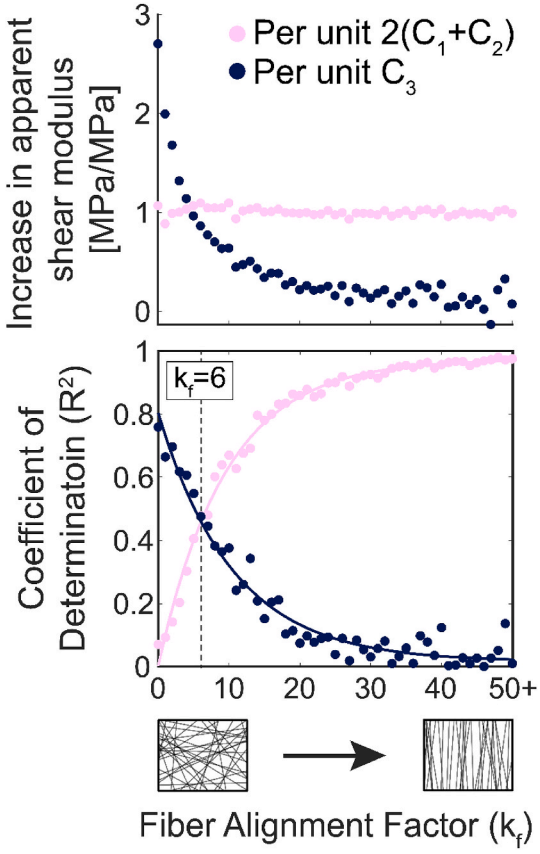

Fig. 6. (top) The ground matrix shear modulus was on average a constant predictor of the tissue's apparent shear modulus (average slope = 1.07 MPa/MPa across all fiber alignment factor values). (bottom) We observed that the exponential stress coefficient, C_3, described more of the variability in apparent shear modulus of the tissue for fiber alignment factor values less than $k_f = 6$.

were better predictors of the apparent shear modulus for a fiber alignment factor, k_f, higher than 6 (Fig. 6). However, the fiber exponential stress coefficient, C_3, was the more dominant predictor of the apparent shear modulus for a fiber alignment factor, k_f, lower than 6.

3.3. Sensitivity of shear wave speed-stress relationship

The slope of the c^2-σ relationship was highly sensitive to the effective tissue density ($R^2 = 0.99$) for both the perfectly aligned and distributed fiber models (Fig. 7i). We also detected a significant increasing relationship between the magnitude of the intercept of the c^2-σ relationship and the stiffness of the ground matrix (C_1, Fig. 7ii) for both model groups ($R^2 = 0.89$ and $R^2 = 0.83$, respectively). We detected that the magnitude of the intercept term also increased with an increase in the exponential stress coefficient, C_3 (Fig. 7iv), for the distributed fiber model only ($R^2 = 0.74$). Other constitutive properties only changed the shear wave speed to the extent that they scaled the axial stress of the model. In the distributed fiber model, the fiber alignment factor and shear wave speed squared-stress slope and intercept were not correlated.

We evaluated the capacity to predict axial stress from shear wave speed using the tensioned beam model (Eq. (7)), with tissue density and unloaded apparent shear modulus taken from the finite element model. For the models with perfectly aligned fibers, there was a strong one-to-one correspondence between the predicted (σ_A) and simulated (σ_{FE}) stress (Fig. 8). The inclusion of distributed fibers tended to result in a slight over-prediction of the tissue stress.

4. Discussion

The objectives of this study were to (1) characterize changes in the apparent shear modulus induced by variations in constitutive properties and fiber alignment, and (2) determine the sensitivity of the shear wave speed-stress relationship to variations in constitutive properties and tissue fiber alignment. The first key finding was that non-aligned fibers increased the model's apparent shear modulus and resulted in an increased in shear wave propagation speed. The second key finding was that the slope, intercept, and predictive ability of the analytical shear wave speed-stress relationship were sensitive to constitutive properties and fiber alignment.

Regarding the first key finding, the apparent shear modulus was strongly dependent on the fiber distribution (Fig. 5). In general, the results showed that, when fibers were aligned with the loading direction (i.e., high k_f), the ground matrix properties were a good predictor of the apparent shear modulus. This result is consistent with transversely isotropic material behavior, in which the long-axis fibers do not stretch during shear deformation and thus do not affect the shear stiffness of the material (Gardiner and Weiss, 2001), (Murphy, 2013). However, as fibers become less well-aligned, the fibers do contribute to the transverse material properties (i.e., stiffness in the x-direction and XZ-plane, Fig. 1), and therefore contribute to the apparent shear modulus. This was directly reflected via the sensitivity of the apparent shear modulus to the exponential stress coefficient, C_3, at low fiber alignment (i.e., $k_f < 6$, Fig. 6), where a 1-MPa increase in the C_3 increased the apparent shear modulus by as much as 4.5 MPa. On the other hand, the apparent shear modulus was insensitive to changes in C_3 when fibers became more highly aligned. It is feasible that similar changes in material anisotropy due to microstructure occur in biological tissues. It is known that ligaments exhibit less aligned fibers than tendons (Amis, 1998), and ligaments in the bovine hoof have been shown to have a similar distribution of fibers to those in our study in the longitudinal direction (average $k_f = 5.7$ using a von Mises distribution) (Stender et al., 2018). Hence, changes in the apparent shear modulus could occur in select tissues with less well-aligned fibers, such as in ligaments (Amis, 1998), (Stender et al., 2018), and similarly, the joint capsule (Bey et al., 2005), (Gohlke

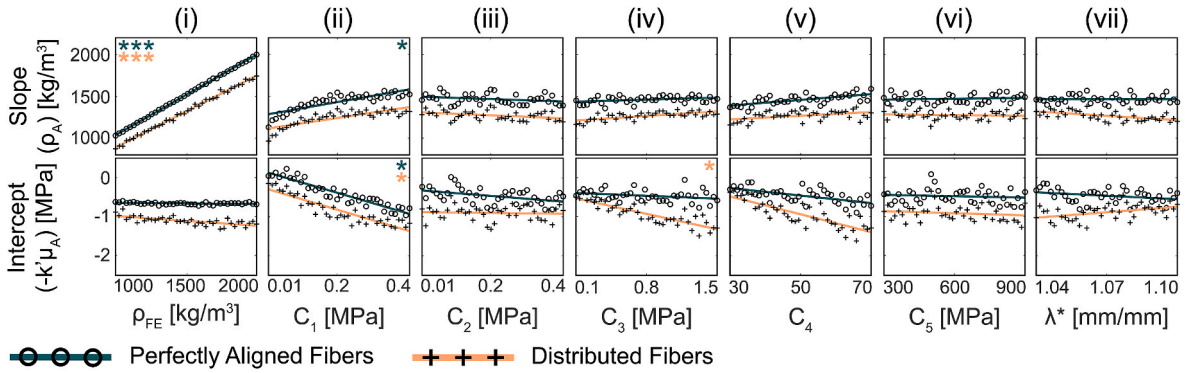

Fig. 7. The sensitivity of the fitted slope (top) and intercept (bottom) of the analytical relationship (Eq. (7)) (ρ_A (i.e., density) and $-k'\mu_A$ (i.e., unloaded apparent shear modulus), respectively), to finite element model constitutive parameters was assessed across 40 separate bins composed of 250 models each. Asterisks indicate the strength of a linear fit (* = $R^2 > 0.7$, ** = $R^2 > 0.9$, *** = $R^2 > 0.99$).

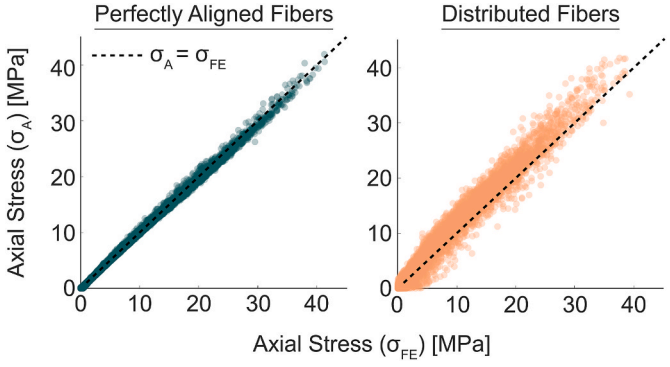

Fig. 8. (left) The tensioned beam model predictions of axial stress agreed well with the measured axial stress for the models with perfectly aligned fibers (average RMSE = 0.34 MPa). (right). In contrast, for the distributed fiber model, the axial stress predicted using the tensioned beam model was greater than the measured axial stress (average RMSE = 1.86 MPa). The dashed line represents a unity line where the tensioned beam model-predicted axial stress is equal to the finite element model-measured axial stress.

et al., 1994).

Regarding the second key finding, the simulated relationship between shear wave speed and axial stress was generally consistent with a simple tensioned beam model (Martinet al., 2018) for tissues with highly aligned fibers. Further, shear wave speeds measured using the finite element model were in range with those from previous tensiometry studies, where shear wave speeds ranged from 20 to 90 m/s in tendons (Martin et al., 2019) and from 20 to 160 m/s in ligaments (Blank et al., 2020a) during tensile loading with axial stresses ranging from 0 to 10 MPa. The c^2-σ relationship was highly linear ($R^2 = 0.99$), with the slope of this relationship well represented by the density of the model (Fig. 7i). The y-intercept, or unloaded apparent shear modulus, was primarily determined by the C_1 term, which governs the elasticity of the ground matrix (Fig. 7ii). Therefore, the tensioned beam model well predicted the axial stress of the transversely isotropic tissue, and these predictions were only sensitive to changes in constitutive properties to the extent that they changed the axial stress of the model. This is an important finding because it reveals that variations in constitutive properties, which are commonly seen from subject-to-subject or specimen-to-specimen, are not enough to cause systematic changes in shear wave speed that would in turn introduce errors when predicting axial stress. Only microstructural variations that changed the apparent shear modulus of the finite element model were enough to alter shear wave speeds and their relationship to the axial stress in a manner that was not predicted by the model. Finally, there was a consistent bias between the perfectly aligned fiber model and the distributed fiber model for both slope and intercept predictions. This bias is an effect of the influence of distributed fibers on the apparent shear modulus, where an increase in the intercept (and thus apparent shear modulus) caused a decrease in the predicted slope for shear wave speeds that were similar in magnitude. However, the general trends observed still provide important context into the effect of individual constitutive parameters on terms governing the tensioned beam model.

The effect of fiber alignment on shear wave speeds differed based on the axial load. At low axial stresses, shear wave speeds for models with less well-aligned fibers were higher than those with perfectly aligned fibers. This increase is likely caused by the increase in the model's apparent shear modulus caused by increasingly less well-aligned fibers (Fig. 5). This increase in shear wave speeds in models with distributed fibers is similar to the increase in shear wave speed with increasing fiber stretch shown previously in bulk transversely isotropic materials (Tweten et al., 2015). As the model is loaded further, the fibers stretch, and the contribution of off-axis fibers to the strain energy density function is scaled according to a 2D unimodal distribution function (Eq. (6)). In general, as a biological tissue with highly aligned collagen fibers is axially stretched, there is relatively less engagement of the collagen fibers in shear in comparison to a tissue with an isotropic fiber distribution, as evidenced by less realignment of fibers oriented in the direction of loading (Lake et al., 2012). Further, the ground matrix shear modulus is the primary material governing the shear modulus when fibers are aligned in the loading direction (Gardiner and Weiss, 2001). Thus, for this particular case, there is relatively little change in the tissue's apparent shear modulus, which is already relatively low in magnitude (less than 1.6 MPa) (Weiss et al., 2002), (Tanakaet al., 2007). Therefore, when the tissue is loaded, the axial stress becomes the dominant term in the equation relating the shear wave speed to axial stress and apparent shear modulus (Eq. (7)). However, less well-aligned fibers may cause a load-dependent increase in the apparent shear modulus as fibers out of alignment with the loading direction are stretched (see Supplementary material Fig. S5.1), which may cause a slight overprediction of the tissue's axial stress (as observed in Fig. 8) due to a calibration using the intercept of the c^2-σ relationship (i.e., unloaded apparent shear modulus). Future studies will be designed to investigate whether an increase in the microstructure-dependent apparent shear modulus with load in tissues with less well-aligned fibers is sufficiently high to change the relationship between the shear wave speed and axial stress with increasing tissue strain.

The approach used in this study has limitations to consider when interpreting the results. In this study, we implemented a 2D fiber distribution to determine its effect on the measured shear wave speed. It is possible that, in tendon and ligament, fibers are just as likely to be distributed in any orientation about the longitudinal axis (i.e., a 3D fiber distribution). However, we chose to use a 2D fiber distribution in the present study because, in our preliminary work, we did not observe

changes in the c^2-σ relationship when the 2D fiber distribution was in a plane whose normal was parallel to the tap direction (i.e., YZ plane in Fig. S1, Supplementary material S3). This finding is in agreement with Shcherbakova et al. who also determined that the shear wave speed did not vary due to fiber orientation or fiber dispersion (i.e., distribution) when fibers were distributed out-of-plane with the shear wave (Shcherbakovaet al., 2017). Thus, we likely captured the greatest effects of fiber alignment on shear wave propagation with fibers distributed in planes parallel to the tap.

A second limitation is that our model cannot account for additional mechanisms that may modulate the fiber-dependent material properties of connective tissue *in vivo*, such as interfibrillar shear (Szczesny and Elliott, 2014), non-affine fiber kinematics (Lake et al., 2012), (Dhume and Barocas, 2019), (Chandran and Barocas, 2006), and orientation-dependent shear wave propagation (Brum et al., 2014), (Aubryet al., 2013), (Royer et al., 2011). Some of these mechanisms are known to change the shear engagement of collagen fibers during axial loading and contribute to the nonlinear response of tendon or ligament to shear, and thus may modulate the effect of less well-aligned fibers on the apparent shear modulus of a tissue. Further, kinematic fiber affinity is an assumption in our finite element model and an inherent assumption in many constitutive models, and we expect that a biological tissue with non-affine fiber kinematics may further complicate the relationship between axial load and microstructure-dependent shear modulus. Finally, shear wave speeds in the unloaded Achilles tendon are different when measured perpendicular to the fibers rather than parallel to fibers (Brum et al., 2014), (Aubryet al., 2013), which suggests there is anisotropy within the tissue. Our finite element model does not capture this anisotropy, with the isotropic ground matrix exhibiting a shear modulus that was the same in all three planes (Fig. 1).

A third limitation is that we only analyzed shear wave propagation under pure, uniform, axial loading conditions. Non-uniform loading could give rise to substantial shear deformations, which could further alter the apparent shear modulus of the material. Thus, our findings may be conservative especially in tissues such as the medial collateral ligament that are frequently loaded non-uniformly in situ and are often under small axial loads. In such tissues, accounting for increases in apparent shear modulus may be important for accurate predictions of axial stress from measured shear wave speeds.

It has previously been shown that guided wave behavior can arise in tendons due to the finite thickness of the tissue, and thereby can alter the relationship between tissue material properties and shear wave speed (Helfenstein-Didieret al., 2016), (Dhume and Barocas, 2019). We did not incorporate analysis methods to account for guided wave effects but did utilize the same excitation and analysis methods between models to enable consistent evaluation of the effects of loading levels, constitutive properties, and fiber alignment.

Finally, while many finite element models have been implemented to study shear wave propagation ,(Caenen et al., 2020), (Palmeri et al., 2005), (Palmeri et al., 2017), (Sadeghi and Cortes, 2019), the primary purpose of this study was to use this dynamic model to study the shear wave speed-stress relationship that governs tensiometry. We found that transient shear wave speeds measured in our finite element model are consistent with those predicted using a simple tensioned beam model (Martinet al., 2018). However, the full richness of this dynamic finite element modeling technique remains to be studied. Future work should leverage this finite element model to study a range of physical phenomena in soft tissues (e.g., guided wave behavior, viscoelasticity, geometry) and their effect on shear wave propagation.

In summary, we used a dynamic finite element model to study the effects of material and microstructural properties on shear wave propagation. This study elucidated important relationships between microstructure and material properties. Our key findings suggest that (1) non-aligned fibers increased the model's apparent shear modulus, which causes an increase in shear wave propagation speed, and (2) the slope, intercept, and predictive ability of the analytical shear wave speed-stress relationship is sensitive to constitutive properties and fiber alignment. Further, the relationship between the shear wave speed and axial stress was sensitive to fibers that are less well-aligned to the loading direction due to increased material isotropy in the plane of the shear wave. More broadly, this study presented a high-throughput, dynamic finite element modeling framework that can be used to study shear wave propagation and tissue structure-function relationships and can be further used to identify cause-effect relationships in experimental tensiometry data.

CRediT authorship contribution statement

Jonathon L. Blank: Conceptualization, Methodology, Software, Validation, Formal analysis, Resources, Data curation, Writing – original draft, Visualization. **Darryl G. Thelen:** Conceptualization, Writing – review & editing, Supervision, Funding acquisition. **Matthew S. Allen:** Conceptualization, Writing – review & editing, Supervision. **Joshua D. Roth:** Conceptualization, Writing – review & editing, Supervision, Project administration, Funding acquisition.

Declaration of competing interest

The authors declare that they have no known competing financial interests or personal relationships that could have appeared to influence the work reported in this paper.

Acknowledgments

We would like to thank the University of Wisconsin-Madison Center for High-Throughput Computing for their technical advice in creating the framework for executing simulations in this study.

This work was supported by the National Institute of Biomedical Imaging and Bioengineering (NIBIB) of the National Institutes of Health under award number [NIBIB: R21EB024957].

This material is based upon work supported by the National Science Foundation Gradudate Research Fellowship under Grant No. DGE-1747503. Any opinions, findings, and conclusions or recommendations expressed in this material are those of the author(s) and do not necessarily reflect the views of the National Science Foundation.

Appendix A. Supplementary data

Supplementary data to this article can be found online at https://doi.org/10.1016/j.jmbbm.2021.104964.

References

Amis, A.A., 1998. "Biomechanics of Bone, Tendon, and Ligament," in *Sciences Basic To Orthopaedics*, pp. 222–239.

Arya, S., Kulig, K., 2010. Tendinopathy alters mechanical and material properties of the Achilles tendon. J. Appl. Physiol. 108 (3), 670–675. https://doi.org/10.1152/japplphysiol.00259.2009.

Aubry, S., et al., 2013. Biomechanical properties of the calcaneal tendon in vivo assessed by transient shear wave elastography. Skeletal Radiol. 42 (8), 1143–1150. https://doi.org/10.1007/s00256-013-1649-9.

Bey, M.J., Hunter, S.A., Kilambi, N., Butler, D.L., Lindenfeld, T.N., 2005. Structural and mechanical properties of the glenohumeral joint posterior capsule. J. Shoulder Elbow Surg. 14 (2), 201–206. https://doi.org/10.1016/j.jse.2004.06.016.

Blank, J.L., Thelen, D.G., Roth, J.D., 2020a. Shear wave speeds track axial stress in porcine collateral ligaments. J. Mech. Behav. Biomed. Mater. 105 (January), 103704. https://doi.org/10.1016/j.jmbbm.2020.103704.

Blank, J.L., Thelen, D.G., Roth, J.D., 2020b. Ligament shear wave speeds are sensitive to tensiometer-tissue interactions: a parametric modeling study. Comput. Methods, Imaging Vis. Biomech. Biomed. Eng. Sel. Pap. from 16th Int. Symp. C. 4th Conf. Imaging Vis. August 14-16, 2019, New York City, USA 36, 48–59.

Brum, J., Bernal, M., Gennisson, J.L., Tanter, M., Feb. 2014. In vivo evaluation of the elastic anisotropy of the human Achilles tendon using shear wave dispersion analysis. Phys. Med. Biol. 59 (3), 505–523. https://doi.org/10.1088/0031-9155/59/3/505.

Burks, R., Haut, R., Lancaster, R., 1990. Biomechanical assessment of the healing response of the rabbit patellar tendon after removal of its central third. Am. J. Sports Med. 18 (2), 146–152. https://doi.org/10.1007/BF00387577.

Caenen, A., Knight, A.E., Rouze, N.C., Bottenus, N.B., Segers, P., Nightingale, K.R., 2020. Analysis of multiple shear wave modes in a nonlinear soft solid: experiments and finite element simulations with a tilted acoustic radiation force. J. Mech. Behav. Biomed. Mater. 107 (March), 103754. https://doi.org/10.1016/j.jmbbm.2020.103754.

Cespedes, I., Huang, Y., Ophir, J., Spratt, S., 1995. Methods for estimation of subsample time delays of digitized echo signals. Ultrason. Imag. 17 (2), 142–171. https://doi.org/10.1006/uimg.1995.1007.

P. L. Chandran and V. H. Barocas, "Affine versus non-affine fibril kinematics in collagen networks: theoretical studies of network behavior," J. Biomech. Eng., vol. 128, no. 2, pp. 259–270, Apr. 2006, doi: 10.1115/1.2165699.

Corrigan, P., Zellers, J.A., Balascio, P., Silbernagel, K.G., Cortes, D.H., 2019. Quantification of mechanical properties in healthy Achilles tendon using continuous shear wave elastography: a reliability and validation study. Ultrasound Med. Biol. 45 (7), 1574–1585. https://doi.org/10.1016/j.ultrasmedbio.2019.03.015.

Cortes, D.H., Suydam, S.M., Silbernagel, K.G., Buchanan, T.S., Elliott, D.M., 2015. Continuous shear wave elastography: a new method to measure viscoelastic properties of tendons in vivo. Ultrasound Med. Biol. 41 (6), 1518–1529. https://doi.org/10.1016/j.ultrasmedbio.2015.02.001.

Crameri, F., Shephard, G.E., Heron, P.J., 2020. The misuse of colour in science communication. *Nat. Commun.*, no. V (–10), 1. https://doi.org/10.1038/s41467-020-19160-7.

Dhume, R.Y., Barocas, V.H., 2019. Emergent structure-dependent relaxation spectra in viscoelastic fiber networks in extension. Acta Biomater. 87, 245–255. https://doi.org/10.1016/j.actbio.2019.01.027.

S. B. Dong, C. Alpdogan, and E. Taciroglu, "Much ado about shear correction factors in Timoshenko beam theory," Int. J. Solid Struct., vol. 47, no. 13, pp. 1651–1665, Jun. 2010, doi: 10.1016/j.ijsolstr.2010.02.018.

Gardiner, J.C., Weiss, J.A., 2001. Simple shear testing of parallel-fibered planar soft tissues. J. Biomech. Eng. 123 (2), 170–175. https://doi.org/10.1115/1.1351891.

Gardiner, J.C., Weiss, J.A., 2003. Subject-specific finite element models can predict strain in the human medial collateral ligament. J. Orthop. Res. 21, 1098–1106. https://doi.org/10.1016/S0736-0266(03)00113-X.

Girard, M.J.A., Downs, J.C., Burgoyne, C.F., Suh, J.-K.F., May 2009. Peripapillary and posterior scleral mechanics—Part I: development of an anisotropic hyperelastic constitutive model. J. Biomech. Eng. 131 (5), 1–9. https://doi.org/10.1115/1.3113682.

Gohlke, F., Essigkrug, B., Schmitz, F., 1994. The pattern of the collagen fiber bundles of the capsule of the glenohumeral joint. J. Shoulder Elbow Surg. 3 (3), 111–128. https://doi.org/10.1016/S1058-2746(09)80090-6.

Gouget, C.L.M., Girard, M.J., Ethier, C.R., 2012. A constrained von Mises distribution to describe fiber organization in thin soft tissues. Biomech. Model. Mechanobiol. 11 (3–4), 475–482. https://doi.org/10.1007/s10237-011-0326-y.

Helfenstein-Didier, C., et al., 2016. In vivo quantification of the shear modulus of the human Achilles tendon during passive loading using shear wave dispersion analysis. Phys. Med. Biol. 61, 2485–2496.

Kannus, P., 2000. Structure of the Tendon Connective Tissue, pp. 312–320, 3.

Lake, S.P., Cortes, D.H., Kadlowec, J.A., Soslowsky, L.J., Elliott, D.M., 2012. Evaluation of affine fiber kinematics in human supraspinatus tendon using quantitative projection plot analysis. Biomech. Model. Mechanobiol. 11 (1–2), 197–205. https://doi.org/10.1007/s10237-011-0303-5.

Maas, S.A., Ellis, B.J., Ateshian, G.A., Weiss, J.A., 2012. FEBio: finite element for biomechanics. J. Biomech. Eng. 134 (1), 011005: 1–10.

Martin, J.A., Schmitz, D.G., Ehlers, A.C., Allen, M.S., Thelen, D.G., 2019. Calibration of the shear wave speed-stress relationship in ex vivo tendons. J. Biomech. 90, 9–15. https://doi.org/10.1016/j.jbiomech.2019.04.015.Calibration.

Martin, J.A., et al., 2018. Gauging force by tapping tendons. Nat. Commun. 9 (1), 2–10. https://doi.org/10.1038/s41467-018-03797-6.

Murphy, J.G., 2013. Transversely isotropic biological, soft tissue must be modelled using both anisotropic invariants. Eur. J. Mech. Solid. 42, 90–96. https://doi.org/10.1016/j.euromechsol.2013.04.003.

Palmeri, M.L., Sharma, A.C., Bouchard, R.R., Nightingale, R.W., Nightingale, K.R., 2005. A finite-element method model of soft tissue response to impulsive acoustic radiation force. IEEE Trans. Ultrason. Ferroelectrics Freq. Control 52 (10), 1699–1712. https://doi.org/10.1109/TUFFC.2005.1561624.

Palmeri, M.L., Qiang, B., Chen, S., Urban, M.W., 2017. Guidelines for finite-element modeling of acoustic radiation force-induced shear wave propagation in tissue-mimicking media. IEEE Trans. Ultrason. Ferroelectrics Freq. Control 64 (1), 78–92. https://doi.org/10.1109/TUFFC.2016.2641299.

Provenzano, P.P., Vanderby, R., 2006. Collagen fibril morphology and organization: implications for force transmission in ligament and tendon. Matrix Biol. 25 (2), 71–84. https://doi.org/10.1016/j.matbio.2005.09.005.

Quapp, K.M., Weiss, J.A., 1998. Material characterization of human medial collateral ligament. J. Biomech. Eng. 120 (6), 757. https://doi.org/10.1115/1.2834890.

Reeves, N.D., Maganaris, C.N., Narici, M.V., 2003. Effect of strength training on human patella tendon mechanical properties of older individuals. J. Physiol. 548 (3), 971–981. https://doi.org/10.1113/jphysiol.2002.035576.

Reeves, N.D., Maganaris, C.N., Maffulli, N., Rittweger, J., 2009. Human patellar tendon stiffness is restored following graft harvest for anterior cruciate ligament surgery. J. Biomech. 42 (7), 797–803. https://doi.org/10.1016/j.jbiomech.2009.01.030.

Royer, D., Gennisson, J.-L., Deffieux, T., Tanter, M., 2011. On the elasticity of transverse isotropic soft tissues (L). J. Acoust. Soc. Am. 129 (5), 2757–2760. https://doi.org/10.1121/1.3559681.

Sadeghi, S., Cortes, D.H., October 2019. Measurement of the shear modulus in thin-layered tissues using numerical simulations and shear wave elastography. J. Mech. Behav. Biomed. Mater. 102, 2020. https://doi.org/10.1016/j.jmbbm.2019.103502.

Shcherbakova, D.A., et al., 2017. A finite element model to study the effect of tissue anisotropy on ex vivo arterial shear wave elastography measurements. Phys. Med. Biol. 62 (13), 5245–5275. https://doi.org/10.1088/1361-6560/aa7125.

Shrive, N., Chimich, D., Marchuk, L., Wilson, J., Brant, R., Frank, C., 1995. Soft-tissue 'flaws' are associated with the material properties of the healing rabbit medial collateral ligament. J. Orthop. Res. 13 (6), 923–929. https://doi.org/10.1002/jor.1100130617.

Sivaguru, M., et al., 2010. Quantitative analysis of collagen fiber organization in injured tendons using Fourier transform-second harmonic generation imaging. Opt Express 18 (24), 24983. https://doi.org/10.1364/oe.18.024983.

Stender, C.J., Rust, E., Martin, P.T., Neumann, E.E., Brown, R.J., Lujan, T.J., 2018. Modeling the effect of collagen fibril alignment on ligament mechanical behavior. Biomech. Model. Mechanobiol. 17 (2), 543–557. https://doi.org/10.1007/s10237-017-0977-4.

Szczesny, S.E., Elliott, D.M., 2014. Interfibrillar shear stress is the loading mechanism of collagen fibrils in tendon. Acta Biomater. 10 (6), 2582–2590. https://doi.org/10.1016/j.actbio.2014.01.032.

Tanaka, E., et al., 2007. Dynamic shear properties of the porcine molar periodontal ligament. J. Biomech. 40 (7), 1477–1483. https://doi.org/10.1016/j.jbiomech.2006.06.022.

Timoshenko, S.P., May 1921. "LXVI. On the correction for shear of the differential equation for transverse vibrations of prismatic bars. London, Edinburgh, Dublin Philos. Mag. J. Sci. 41 (245), 744–746. https://doi.org/10.1080/14786442108636264.

S. P. Timoshenko, "X. On the transverse vibrations of bars of uniform cross-section," London, Edinburgh, Dublin Philos. Mag. J. Sci., vol. 43, no. 253, pp. 125–131, Jan. 1922, doi: 10.1080/14786442208633855.

Tweten, D.J., Okamoto, R.J., Schmidt, J.L., Garbow, J.R., Bayly, P.V., 2015. Estimation of material parameters from slow and fast shear waves in an incompressible, transversely isotropic material. J. Biomech. 48 (15), 4002–4009. https://doi.org/10.1016/j.jbiomech.2015.09.009.

Waugh, C.M., Blazevich, A.J., Fath, F., Korff, T., 2012. Age-related changes in mechanical properties of the Achilles tendon. J. Anat. 220 (2), 144–155. https://doi.org/10.1111/j.1469-7580.2011.01461.x.

Weiss, J., Maker, B., Govindjee, S., 1996. Finite Element Implementation of Incompressible, Transversely Isotropic Hyperelasticity, pp. 107–128.

Weiss, J.A., Gardiner, J.C., Bonifasi-Lista, C., 2002. Ligament material behavior is nonlinear, viscoelastic and rate-independent under shear loading. J. Biomech. 35 (7), 943–950. https://doi.org/10.1016/S0021-9290(02)00041-6.

Woo, S.L., Orlando, C.A., Gomez, M.A., Frank, C.B., Akeson, W.H., 1986. Tensile properties of the medial collateral ligament as a function of age. J. Orthop. Res. 4 (2), 133–141. https://doi.org/10.1002/jor.1100040201.

Wu, J., Qian, Z., Liang, W., Liu, J., Ren, L., Ren, L., 2020. In vivo assessment of material properties of muscles and connective tissues around the knee joint based on shear wave elastography. J. Mech. Behav. Biomed. Mater. 109 (April), 103829. https://doi.org/10.1016/j.jmbbm.2020.103829.